Theoretical and Applied Climatology (2019) 135:391–408
https://doi.org/10.1007/s00704-018-2371-2

ORIGINAL PAPER

Spatiotemporal variation and statistical characteristic of extreme precipitation in the middle reaches of the Yellow River Basin during 1960–2013

Yin Zhang[1] · Jun Xia[1,2] · Dunxian She[1]

Received: 27 September 2017 / Accepted: 3 January 2018 / Published online: 27 January 2018

Abstract
In recent decades, extreme precipitation events have been a research hotspot worldwide. Based on 12 extreme precipitation indices, the spatiotemporal variation and statistical characteristic of precipitation extremes in the middle reaches of the Yellow River Basin (MRYRB) during 1960–2013 were investigated. The results showed that the values of most extreme precipitation indices (except consecutive dry days (CDD)) increased from the northwest to the southeast of the MRYRB, reflecting that the southeast was the wettest region in the study area. Temporally, the precipitation extremes presented a drying trend with less frequent precipitation events. Generalized extreme value (GEV) distribution was selected to fit the time series of all indices, and the quantiles values under the 50-year return period showed a similar spatial extent with the corresponding precipitation extreme indices during 1960–2013, indicating a higher risk of extreme precipitation in the southeast of the MRYRB. Furthermore, the changes in probability distribution functions of indices for the period of 1960–1986 and 1987–2013 revealed a drying tendency in our study area. Both El Niño–Southern Oscillation (ENSO) and Pacific Decadal Oscillation (PDO) were proved to have a strong influence on precipitation extremes in the MRYRB. The results of this study are useful to master the change rule of local precipitation extremes, which will help to prevent natural hazards caused.

Keywords Extreme precipitation · Extreme distribution · The middle reaches of the Yellow River Basin

1 Introduction

According to the fifth assessment report of the Intergovernmental Panel on Climate Change (IPCC), the global mean surface temperature has increased since the late nineteenth century, with a total increase of about 0.85 °C during 1880–2012 (IPCC, 2013). The global warming can probably strengthen the atmospheric moisture levels, thunderstorm activity, and/or large-scale storm activity, which may result in an increase in the magnitude and frequency of extreme precipitation events (Trenberth, 1998; Sen Roy and Balling, 2004). Studies about extreme precipitation have been carried out in various regions around the world (Alexander et al., 2006), such as southern Brazil (Sansigolo and Kayano, 2010), Japan (Duan et al., 2015), Australia (Fiddes et al., 2014), Thailand (Limsakul and Singhruck, 2016), and Korea (Min et al., 2015). These studies have concluded that the changes in extreme precipitation exhibit large regional variability. For example, significant decreasing trends in extreme precipitation events were observed in some areas of western central Africa (Aguilar et al., 2009), whereas extreme precipitation events were found to become more intense in Thailand (Limsakul and Singhruck, 2016). In China, changes in extreme precipitation also attracted many interests (Zhai et al., 2005; You et al., 2011; Xia et al., 2012). Previous studies indicated large variability of the changes in extreme precipitation in space and time in this country (You et al., 2011; Song et al., 2015; Sun et al., 2016). Decreasing trends can be observed in southwestern China, whereas increasing trends were

✉ Jun Xia
xiajun666@whu.edu.cn

[1] State Key Laboratory of Water Resources and Hydropower Engineering Science, Wuhan University, No. 8 Donghu South Road, Wuhan 430072, People's Republic of China

[2] Key Laboratory of Water Cycle and Related Land Surface Processes, Institute of Geographic Sciences and Natural Resources Research, Chinese Academy of Sciences, Beijing 100101, People's Republic of China

observed in Xinjiang, eastern Tibetan Plateau, northeastern China, and southeastern China (Zhai et al., 2005; You et al., 2011). Moreover, the changes in frequency and intensity of extreme precipitation can usually lead to extreme hydrological events, which can exert significant negative impacts on the social and natural environment (Alexander et al., 2006; Choi et al., 2009; dos Santos et al., 2011). For example, the extreme flooding disaster occurred in the Nenjiang River and the Songhua River in northeastern China and the Yangtze River in southern China in 1998 was induced by extreme precipitation events and resulted in more than 3000 casualties and 3.6 billion dollar economic losses (Zong and Chen, 2000). Hence, the research on changes in extreme precipitation is of great significance to provide a scientific basis to reduce the risk of extreme events.

Statistical models are widely regarded as efficient and useful tools to better understand the changes in extreme events. Various statistical distributions were used to model extreme hydrometeorological series, such as extreme value distributions (Xia et al., 2012; Najafi and Moazami, 2016), extended Burr XII distribution (Shao et al., 2004), and Pearson III distribution (Griffis and Stedinger, 2007). The efficiency of these distributions in modeling the precipitation extremes in China has also been assessed by many previous studies (Su et al., 2009; Yang et al., 2010; Fischer et al., 2012). For example, Fischer et al. (2012) compared the efficiency of the three-parameter gamma (gamma 3), generalized extreme value (GEV), generalized Pareto (GP), and Wakeby distributions in modeling the precipitation extremes in the Zhujiang River Basin and revealed that GEV was the most reliable and robust distribution in their study area. Xia et al. (2012) and Du et al. (2014) used GEV and GP distribution, respectively, to describe the extreme precipitation events in the Huaihe River Basin. The probability distributions can comprehensively describe the statistical characteristic of precipitation extremes and detect the changes of precipitation extremes by their changes (Alexander et al., 2006; Fischer et al., 2012). Furthermore, a deep understanding of the statistical characteristic of precipitation extremes can reflect the changes of risks of extreme events and is useful for the planning of adaption (Fischer et al., 2012).

The present study selected the middle reaches of the Yellow River Basin (MRYRB), which is located in the north of China, as the study area to investigate the spatiotemporal variation and statistical characteristic of extreme precipitation. The daily precipitation observation data at 44 meteorological stations during 1960–2013 was used. To the best of our knowledge, previous studies about in this area were mainly focused on trends of extreme precipitation (Liang et al., 2015; Sun et al., 2016). Given that extreme precipitation can usually result in serious socioeconomic losses and casualties, a comprehensive and further analysis of changes in the extreme precipitation covering spatiotemporal variation and statistical characteristic is quite needed. Furthermore, the relationships between precipitation extremes and large-scale atmospheric circulation in the MRYRB were also explored.

The major objectives of this study are as follows: (1) to identify the extreme precipitation events using various indices at all stations and analyze the changes of these indices in space and time; (2) to investigate the statistical characteristic of extreme precipitation in the MRYRB using several probability distributions; (3) to assess the potential changes of risk of extreme precipitation in various time period and analyze whether the precipitation is getting more extreme in the considered area; and (4) to explore whether there are significant relationships between precipitation extremes and large-scale atmospheric circulation patterns.

The structure of this study is as follows: Sect. 2 presents the used data and methods including the definition of extreme precipitation indices; Sect. 3 shows the results and discussions, followed by the conclusion in Sect. 4.

2 Data and method

2.1 Study area

The MRYRB is located in northern China (103° 58′–113° 40′ E, 33° 39′–40° 34′ N) (Fig. 1), covering an area of about 345,600 km^2. This region belongs to the arid and semi-arid climate zone in China. The long-term mean annual precipitation exhibits large spatial variability, ranging from less than 350 mm in the northwest to more than 800 mm in the southeast of the MRYRB. Precipitation during the flooding season (June to September) accounts for about 70% of the total annual precipitation. The mainstream of the MRYRB flows through the Loess Plateau, which is famous for serious soil erosion problem. The average annual erosion rate is about 2480 t km^{-2} for the whole Yellow River Basin, which is the highest over the world for any large rivers (Shi and Shao, 2000). The native vegetation has mostly been cleared for crop production, causing severe soil erosion, land degradation, and soil fertility loss (Jia et al., 2017).

2.2 Data

In this study, the daily precipitation data at 44 meteorological stations during 1960–2013 were used to analyze the spatiotemporal variability and statistical characteristic of extreme precipitation in the MRYRB. These data were provided by China Meteorological Administration (CMA) with high quality. Daily precipitation datasets may have different degrees of heterogeneity due to changes in relocations, measuring techniques, and environment, which often leads to significant bias in the extreme precipitation trend detection. Therefore, the homogeneity of the datasets should be carefully examined

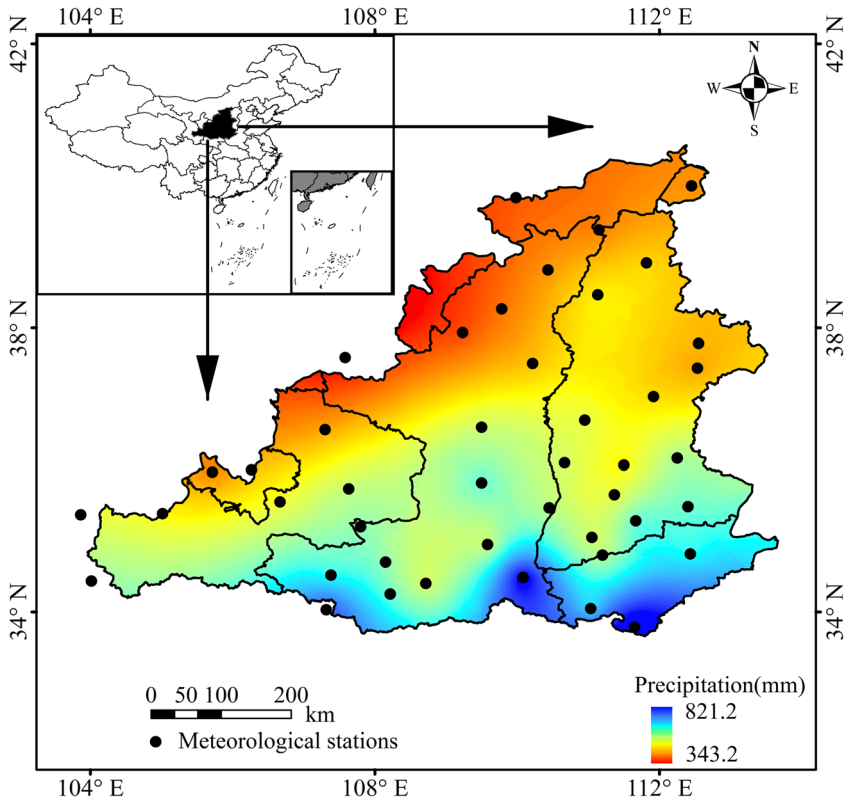

Fig. 1 Spatial distribution of meteorological stations and mean annual precipitation in the MRYRB

before the use of datasets. In this study, the RH test-dlyprcp software, which was developed by Wang and Feng (2013) (available at http://etccdi.pacificclimate.org/software.shtml) specifically for daily precipitation data time series homogeneity test, was employed to check the homogeneity of daily precipitation series in all stations. The results showed that all the daily precipitation series at 44 meteorological stations passed the homogeneity test at the significance level of 0.05, which confirmed their reliability in the extreme precipitation analysis. The regional averages were calculated as arithmetic means of the values at all selected stations in the study area.

To examine the relationships between the precipitation extremes and the large-scale atmospheric circulation patterns, the correlations between the extreme precipitation indices and El Niño–Southern Oscillation (ENSO)/Pacific Decadal Oscillation (PDO) indices were investigated. In this study, the Nino 3.4 index, which is defined as the monthly sea surface temperature averaged over the east central tropical Pacific (5° N–5° S, 170°–120° W), was used to represent the state of ENSO. The monthly PDO index is defined as the leading principal component of North Pacific monthly sea surface temperature variability, which has been proved to be closely related to the variability of extreme precipitation (Limsakul and Singhruck, 2016; Liu et al., 2017). These data were downloaded from the National Oceanic and Atmospheric Administration (NOAA) Earth System Research Laboratory (available online at http://www.esrl.noaa.gov/psd/data/climateindices/list/).

2.3 Method

2.3.1 The definition of extreme precipitation indices

Generally, extreme precipitation events often refer to these precipitation events that occur infrequently but with severe impacts. The Expert Team on Climate Change Detection and Indices (ETCCDI) has defined 27 types of extreme indices, including 11 types of indices about extreme precipitation and 16 types of indices about temperature. The standard indices established by ETCCDI have been widely used to assess climate changes of extreme precipitation in different regions of the world (Alexander et al., 2006; You et al., 2011; Sun et al., 2016). We selected nine of extreme precipitation indices from the ETCCDI to reflect the changes in extreme precipitation intensity, frequency, and duration in the MRYRB. As the study area is frequently attacked by serious drought hazards, which are mostly related to light precipitation (Wu and Qian, 2016), the number of precipitation days (R0.1 mm), which relates to precipitation amount no less than 0.1 mm, was considered. On the other hand, as the erosive rainfall has an evident impact on runoff and soil erosion in the study area, the erosive rainfall should be specifically considered when analyzing the precipitation extremes in the MRYRB. Here, the

threshold of 12 mm/day, which was suggested by Xie et al. (2000) as the standard for describing erosive rainfall on the Loess Plateau, was used. Moreover, the number of heavy precipitation days, which refers to a day with precipitation amount exceeding 25 mm/day defined by the National Climate Center of China, was also considered. To sum up, the foregoing mentioned 12 indices of precipitation extremes can be generally divided into two groups: (1) the indices that describe the precipitation intensity, including SDII, PRCPTOT, R95, R99, RX1day, and RX5day and (2) the indices that reflect the number of precipitation days, including CDD, CWD, R0.1mm, R10mm, R12mm, and R25mm. Detailed descriptions about these indices were provided in Table 1.

2.3.2 Mann-Kendall test

Non-parametric Mann-Kendall (MK) test is a simple and robust trend detection method (Mann, 1945; Kendall, 1975). It is recommended by the World Meteorological Organization (WMO) as a standard procedure for examining trends in independent hydrometeorological series and has been widely used (Gocic and Trajkovic, 2013; She et al., 2016; Yang et al., 2017). In this study, we used the MK test to examine the temporal trends in extreme precipitation indices in the MRYRB.

The MK statistical test is given as follow:

$$Z = \begin{cases} \dfrac{S-1}{\sqrt{Var(S)}} & S > 0 \\ 0 & S = 0 \\ \dfrac{S+1}{\sqrt{Var(S)}} & S < 0 \end{cases} \quad (1)$$

where statistic S can be calculated as:

$$S = \sum_{i=1}^{n-1} \sum_{j=i+1}^{n} \mathrm{sgn}\left(x_j - x_i\right) \quad (2)$$

where x_i and x_j are the observations at the ith and jth moments, respectively; n is the length of the series. When $x_i - x_j$ is more than, equal to or less than 0, $\mathrm{sgn}(x_i - x_j)$ equals to 1, 0, or − 1, respectively.

The statistic Z can be used as a measure of a trend. $Z > 0$ and $Z < 0$ indicate an increasing and decreasing trend, respectively. A larger $|Z|$ value refers to a more significant trend. In this study, the significance level of 0.05 is considered, which means that $Z > 1.96$ and $Z < -1.96$ will indicate a significant increasing and decreasing trend, respectively.

However, many previous studies have stated that the possible existence of autocorrelation in the time series can lead to inaccurate estimation of the trends (Yue and Wang, 2002). Therefore, we should remove the autocorrelation, if it exists, before the application of MK test. In this study, the method given in Yue and Wang (2002) was performed to remove the possible autocorrelation in the extreme precipitation series in the MRYRB.

Moreover, the Sen's slope (Sen, 1968) was also used to determine the magnitude of the trend, as it can eliminate the impact of missing data or anomalies on the trend test. The slope is estimated by

$$\beta = Median\left[\frac{\left(x_j - x_i\right)}{(j-i)}\right], \forall j > i \quad (3)$$

where β is the estimate of the slope of the trend; x_i and x_j are the observations at the ith and jth moments, respectively.

2.3.3 Statistical distribution models

In this study, the statistical characteristic of extreme precipitation was analyzed using the extreme value distributions. Many extreme distributions have been used to simulate the changes in extreme hydrometeorological time series (She et al., 2015; She et al., 2016). Here, the GEV distribution and GP distribution were considered due to their good performance in modeling the extremes (Xia et al., 2012; Fischer et al., 2012; Bhunya et al., 2013). Additionally, given that the gamma distribution has been proved to be the appropriate model for the simulation of precipitation time series in China (Liang et al., 2012; Jiang et al., 2014), this distribution was also used. Therefore, we selected three models to fit the extreme precipitation time series and further analyze the statistical characteristic in the precipitation extremes in our study area. Here, we only gave the description of the three distributions in brevity, which can be seen in Table 2, and the details can be referred to Xia et al. (2012). The parameters of these distributions were estimated using the L-moments method (Hosking, 1990; Hosking and Wallis, 1997). The most prominent feature of L-moments is that it is not so sensitive to the maximum and minimum values compared to ordinary moments, which makes the estimates of parameters by L-moments method are more robust (Cai & Jiang 2007). Besides, the Kolmogorov-Smirnov (KS) test was employed to choose the optimal models. The readers can find the details of the L-moment method in Hosking and Wallis (1997) and the KS test in Young (1977).

2.3.4 Cross wavelet analysis

Wavelet transforms have become a useful tool for investigating local variation in time series and have been widely used in hydrological and climatic time series analysis (She et al., 2016; Yang et al., 2017; Liu et al., 2017). The cross wavelet analysis, introduced by Torrence and Compo (1998), was adopted to understand how the changes of ENSO and PDO can affect the extreme precipitation changes in the MRYRB. The details of cross wavelet analysis are given below.

Table 1 Definitions of the 12 precipitation extreme indices used in this study

Index	Descriptive name	Definition	Units
CDD	Consecutive dry days	Maximum number of consecutive dry days	days
CWD	Consecutive wet days	Maximum number of consecutive wet days	days
PRCPTOT	Wet-day precipitation	Annual total precipitation based wet days	mm
R0.1 mm	Number of precipitation days	Annual count of days when RR ≥ 0.1 mm	days
R10mm	Number of moderate precipitation days	Annual count of days when RR ≥ 10 mm	days
R12mm	Number of erosion precipitation days	Annual count of days when RR ≥ 12 mm	days
R25mm	Number of heavy precipitation days	Annual count of days when RR ≥ 25 mm	days
R95	Very wet day	Annual total precipitation when RR > 95th percentile	mm
R99	Extreme very-wet day	Annual total precipitation when RR > 99th percentile	mm
RX1day	Maximum 1-day precipitation	Annual maximum 1-day precipitation	mm
RX5day	Maximum 5-day precipitation	Annual maximum 5-day precipitation	mm
SDII	Simple daily intensity index	Average precipitation on wet days	mm/day

A dry (or wet) day is defined as the daily precipitation is lower (or no less) than 1 mm/day

"RR" refers to daily precipitation amount

For two time series x_n and y_n, the cross wavelet spectrum is defined as

$$W^{XY} = W^X W^{Y*} \tag{4}$$

where W^X and W^Y represent the wavelet transforms and * denotes the complex conjugation. The cross wavelet power is further defined as $|W^{XY}|$. The complex argument arg(W^{xy}) can be interpreted as the local relative phase between x_n and y_n in time frequency space.

The theoretical distribution of the cross wavelet power of two time series with background power spectra P_k^X and P_k^Y is given in Torrence and Compo (1998) as

$$D\left(\frac{\left|W_n^X(s)W_n^{Y*}(s)\right|}{\sigma_X\sigma_Y} < p\right) = \frac{Z_v(p)}{v}\sqrt{P_k^X P_k^Y} \tag{5}$$

where $Z_v(p)$ is the confidence level associated with the probability p for a probability density function defined by the square root of the product of two χ^2 distributions. In this study, the 5% significance level is calculated using $Z_2(95\%) = 3.999$. The more details of the cross wavelet transforms can be found in Grinsted et al. (2004), and the relevant codes can be downloaded from http://www.pol.ac.uk/home/research/waveletcoherence/ .

3 Results and discussions

3.1 Temporal trends of extreme precipitation

3.1.1 Indices of precipitation intensity

We first analyzed the spatial variation and temporal changes of the indices representing the extreme precipitation intensity (Fig. 2). The Kriging method was employed to interpolate the values into the whole study area by means of the software of ArcGIS. The temporal trends were detected by the MK test with a significance level of 0.05. Besides, we also gave the variation of the regional time series of these six extreme precipitation indices in Fig. 3.

As shown in Fig. 2a, the PRCPTOT values ranged from 334.1 to 809.4 mm across the whole study area. The highest

Table 2 The cumulative distribution function and L-moments estimates of parameters

Distribution	Probability density function	Cumulative distribution function	Indicator amount under return period T year
GEV	$f(x) = \frac{1}{\alpha}\left[1 + k\left(\frac{1}{\alpha}\right)\right]^{-\frac{1}{\alpha}}\exp\left\{-\left[1 + k\left(\frac{1}{\alpha}\right)\right]^{-\frac{1}{\alpha}}\right\}$	$F(x) = \exp\{-[1 + (k(x-\xi))\ /\alpha]^{-1/k}\}\ k\neq 0$	$X_T = \hat{\xi} + \frac{\hat{\alpha}}{\hat{k}}(1-(-\ln(1-1/T))^{\hat{k}})$
GP	$f(x) = \left(\frac{1}{\alpha}\right)\left[1-k\left(\frac{1}{\alpha}\right)\right]^{\frac{1}{\alpha}}$	$F(x) = 1-e^{-y}\ y = \{-\ln[1-k(x-\xi)\ /\alpha]\ /k\ \ k\neq 0$ $(x-\xi)\ /\alpha \qquad k = 0$	$X_T = \hat{\xi} + \frac{\hat{\alpha}}{\hat{k}}(1-(1/T)^{\hat{k}})$
Gamma	$f(x) = \begin{cases} \frac{1}{\beta^\alpha\Gamma(\alpha)}x^{\alpha-1}e^{-x/\beta} & X > 0\ 0 \\ X \le 0 \end{cases}$	$F(x) = \frac{1}{\beta^\alpha\Gamma(\alpha)}\int_0^x x^{\alpha-1}e^{-x/\beta}dx$	$X_T = F^{-1}(F(X_T))$

α, ξ, and k represent the scale, location, and shape parameter of GEV and GP distribution, respectively; and $\hat{\alpha}$, $\hat{\xi}$, and $\hat{k}$ are the estimates of α, ξ, and k, respectively

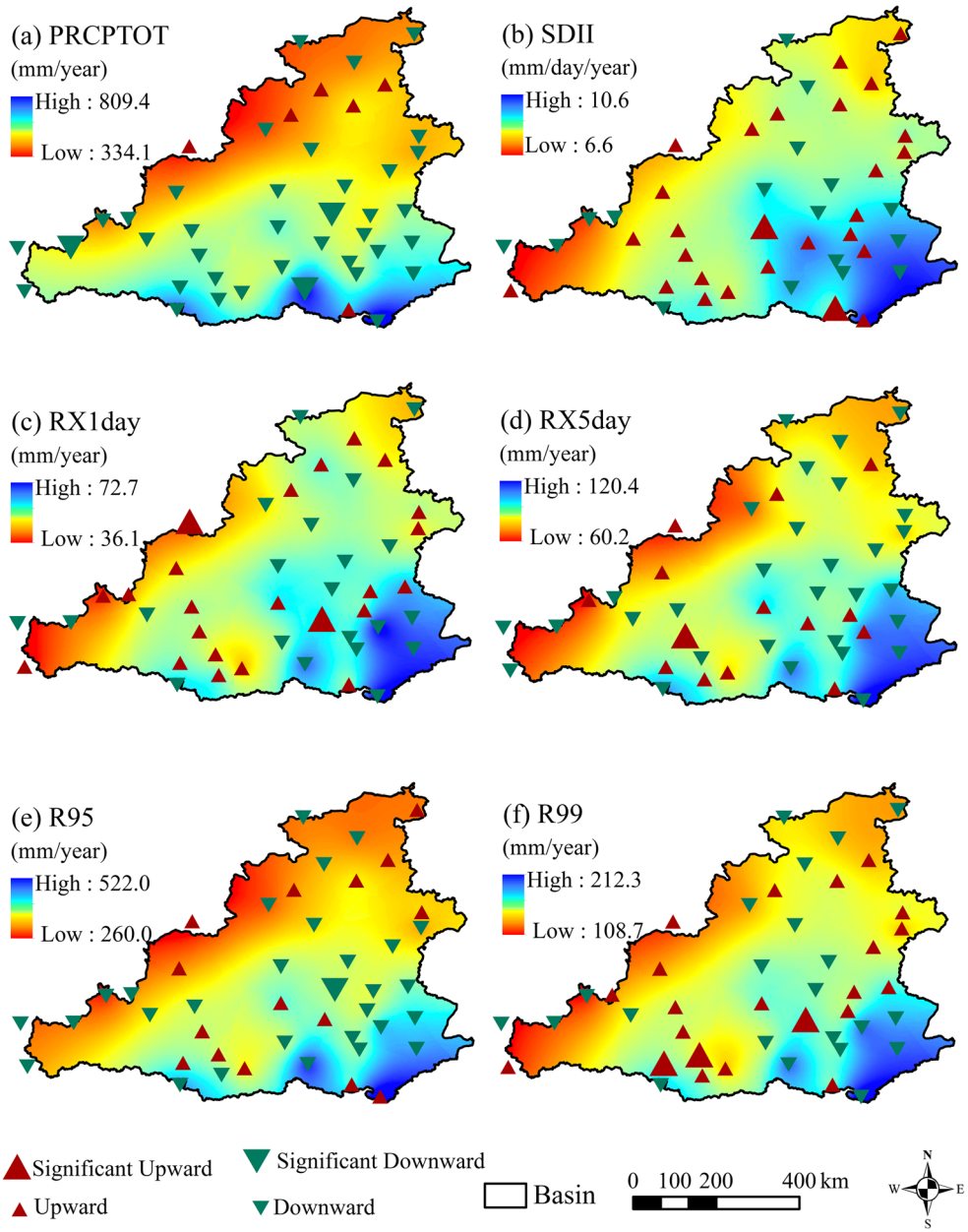

Fig. 2 Spatial patterns of values and trends in indices of precipitation intensity in the MRYRB during 1960–2013. The significance level of 0.05 is considered

value of annual PRCPTOT was distributed in the southeast region while the lowest value appeared in the northwest region, which was consistent with the spatial distribution of annual precipitation in this area (Zhang et al., 2014). Additionally, the spatial patterns of SDII, RX1day, RX5day, R95, and R99 also showed similarities with that of PRCPTOT, that the values increased from the northwest to the southeast of the MRYRB (Fig. 2b–f). The linear correlation coefficients between the regional average time series of each index were calculated to illustrate the relationship between these indices. The PRCPTOT was well correlated (at the 0.01 significance level) with the other five extreme precipitation indices (Table 3). This can partially illustrate the consistency between the spatial variation of the other five indices and PRCPTOT. From the definition of the aforementioned six indices, the higher the index value, the wetter of the climate condition may occur. Therefore, we can infer that the southeast of the MRYRB was the wettest region as all of these six indices were largest in this area, whereas the northwest region was a relatively dry region. On the other hand, considering that the higher the index value (except CDD), the higher risk of occurrence of extreme precipitation, the occurrence probability of extreme precipitation events in the southeast was also higher than that in the northwest region.

Decreasing trends in PRCPTOT can be seen in the majority of stations (38 of 44 stations, 84%) (Fig. 2a), with only three of them was significant. There were only five stations presenting insignificant increasing trends, which were mainly

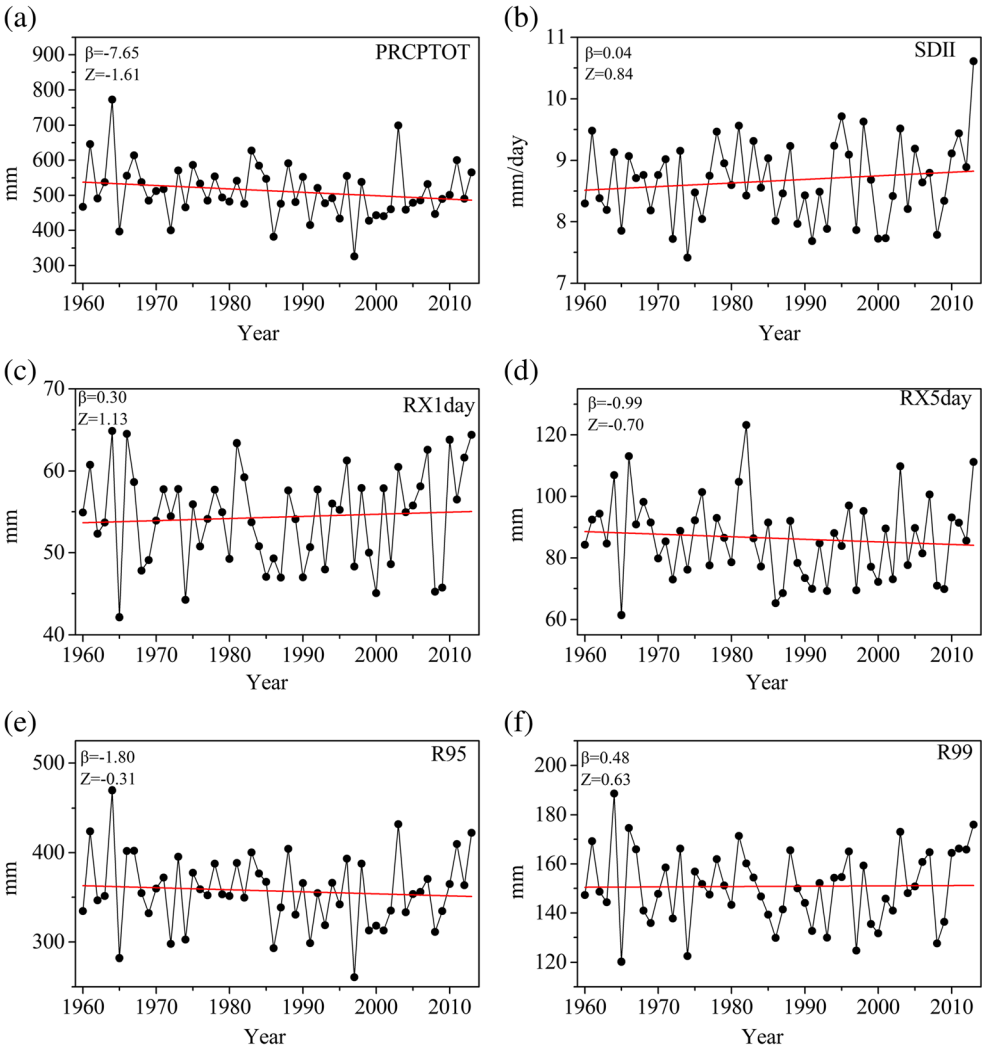

Fig. 3 Regional average series for indices of precipitation intensity in the MRYRB during 1960–2013. The red line represents the slope of the datasets during 1960–2013

distributed in the north of the MRYRB. This can also be seen in the regional average PRCPTOT time series that an insignificant decline trend at a rate of − 7.65 mm/decade can be detected (Fig. 3a). There were 27 and 17 stations that showed increasing and decreasing trends of SDII, respectively (Fig. 2b). Except two stations with significant increasing trends, all of the trends in the other stations were insignificant. Over the whole study area, we found that SDII insignificantly increased at a rate of 0.04 mm/day/decade (Fig. 3b). The combination of the decline in PRCPTOT and increase in SDII at most stations may link to a decrease in the number of wet days, and this will be further discussed in the following section. There were more stations for RX1day showing increasing trends, while much more stations displayed with decreasing trends for RX5day (Fig. 2c and d). Moreover, there were only three stations showing significant increasing trends, two for RX1day and one for RX5day, respectively. Moreover, the regional RX1day and RX5day presented insignificant increasing and decreasing trends during 1960–2013, respectively (Fig. 3c and d). The trends in R95 and R99 also did not show any evident spatial patterns; however, the number of stations giving decreasing trends was larger than that giving increasing trends for R95 (Fig. 2e), whereas more stations showed increasing trends for R99 (Fig. 2f). From the perspective of regional average series, the R95 and R99 also exhibited no significant trend (Fig. 3e and f).

3.1.2 Indices for the number of precipitation days

We analyzed the spatial variation and temporal changes of the indices for the number of precipitation days (Fig. 4) and also gave the temporal variation of the regional time series of these six extreme precipitation indices in Fig. 5.

As shown in Fig. 4a, the CDD values increased from the southeast to the northwest of the MRYRB. The CWD values ranged from 4.0 to 6.4 days/year across the whole study area (Fig. 4b). The highest value of CWD was distributed in the southwest region, while the lowest value appeared in the

Table 3 Correlation coefficient of extreme precipitation indices in the MRYRB during 1960 – 2013

	CDD	CWD	PRCPTOT	R0.1 mm	R10mm	R12mm	R25mm	R95	R99	RX1day	RX5day	SDII
CDD	1											
CWD	− 0.03	1										
PRCPTOT	− 0.11	0.49**	1									
R0.1 mm	− 0.34*	0.49**	0.80**	1								
R10mm	0.02	0.50**	0.97**	0.74**	1							
R12mm	0.02	0.46**	0.96**	0.71**	0.99**	1						
R25mm	− 0.07	0.28*	0.89**	0.55**	0.83**	0.86**	1					
R95	− 0.02	0.38**	0.94**	0.61**	0.89**	0.91**	0.95**	1				
R99	− 0.06	0.24	0.75**	0.43**	0.64**	0.67**	0.86**	0.90**	1			
RX1day	− 0.03	0.14	0.52**	0.25	0.40**	0.42**	0.63**	0.70**	0.92**	1		
RX5day	0.02	0.57**	0.61**	0.38**	0.54**	0.54**	0.60**	0.71**	0.78**	0.73**	1	
SDII	0.30*	0.14	0.59**	0.05	0.61**	0.65**	0.78**	0.79**	0.77**	0.65**	0.60**	1

*Significant at 0.05 level

**Significant at 0.01 level

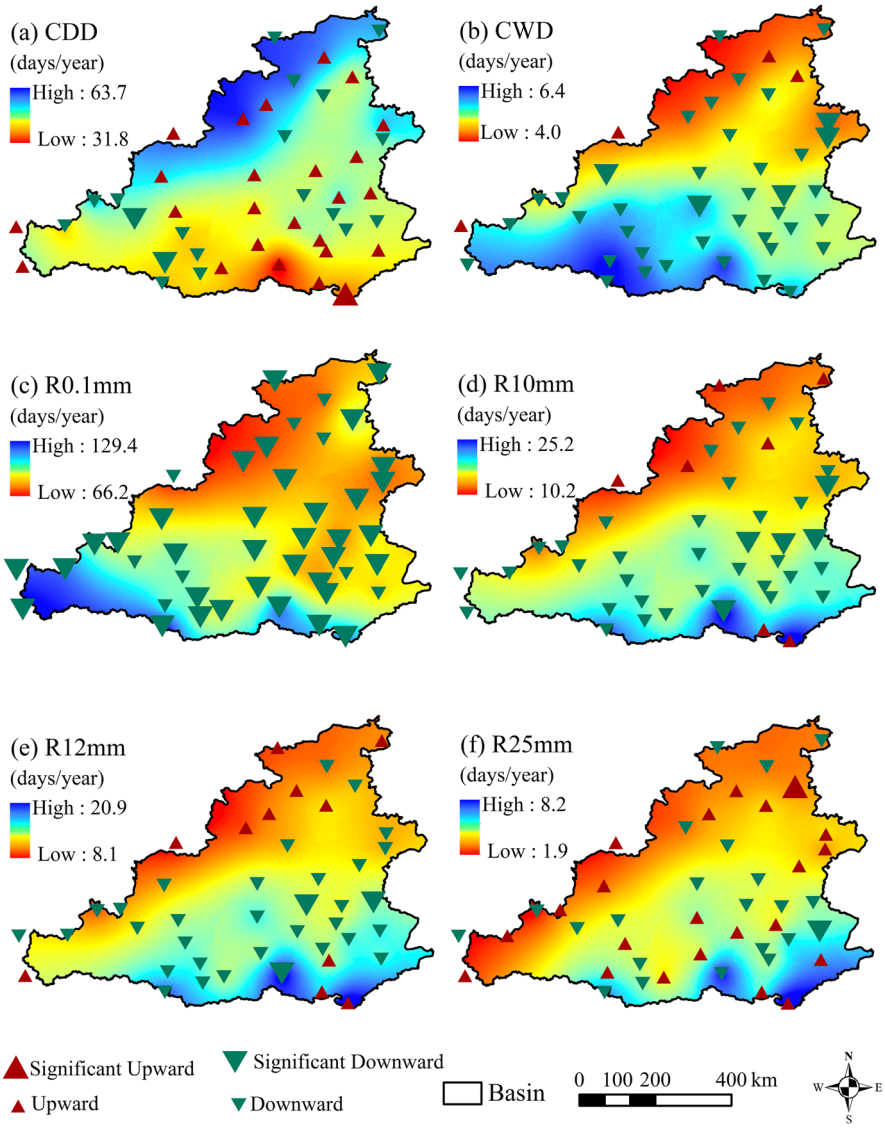

Fig. 4 Spatial patterns of values and trends in indices for the number of precipitation days in the MRYRB during 1960–2013. The significance level of 0.05 is considered

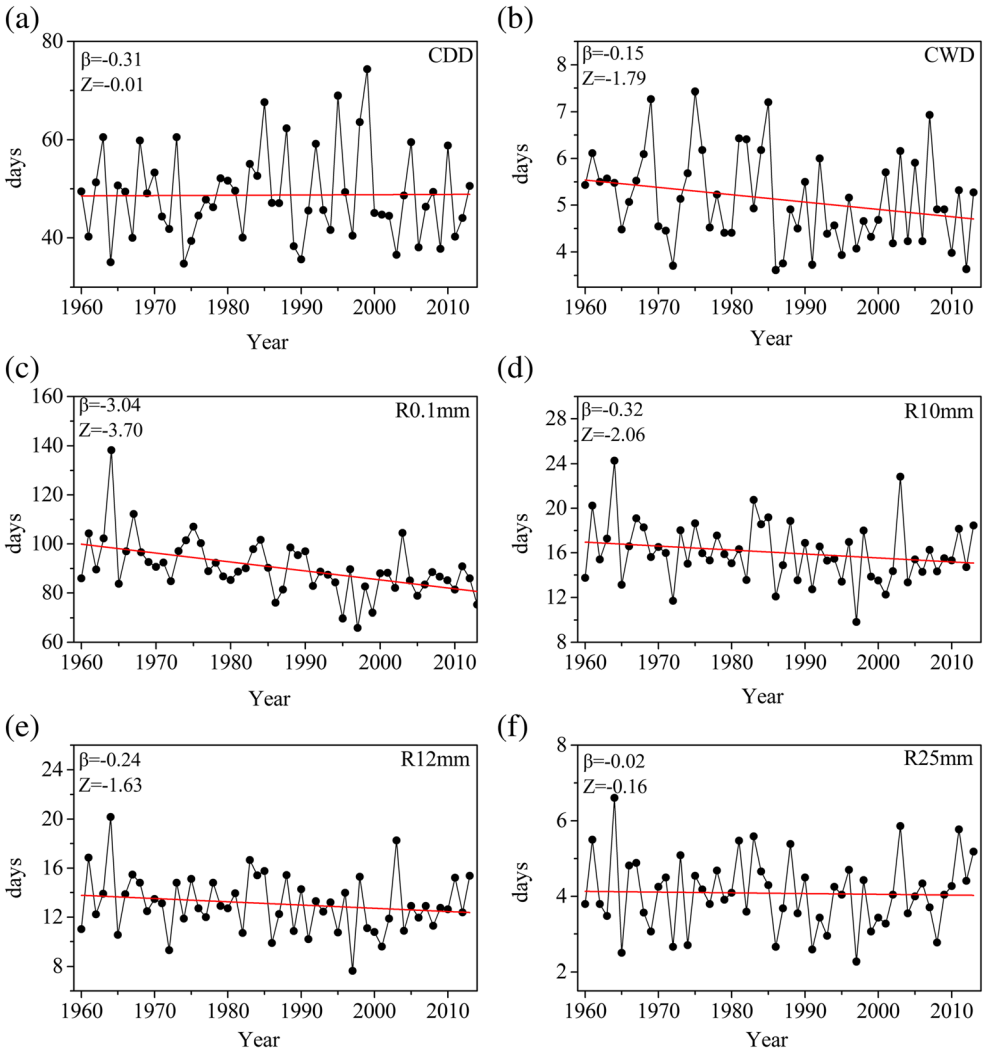

Fig. 5 Regional average series for indices for the number of precipitation days in the MRYRB during 1960–2013. The red line represents the slope of the datasets during 1960–2013

northwest region. The distribution of R0.1mm was quite similar with that of CWD (Fig. 4c), while the highest values of R10mm, R12mm, and R25mm were located in the southeast region (Fig. 4d–f). The similarities and differences in spatial distributions among these indices can be illustrated from the correlation coefficients in Table 3. The correlation coefficients between indices for the number of precipitation days were relatively small (Table 3). For example, the correlation coefficients between CDD and other extreme precipitation indices, except R0.1mm (at the 0.05 significance level), did not pass the 0.05 significance level. From the definition of CWD, R0.1mm, R10mm, R12mm, and R25mm, higher values indicated wetter conditions, whereas lower values suggested drier conditions. Therefore, the spatial distributions of these indices revealed that the southeast of the MRYRB was the relatively wet region as R10mm, R12mm, and R25mm were largest and CDD was smallest in this area, whereas the northwest region was the relatively dry region. On the other hand, the occurrence probability of extreme precipitation events in the southeast was also higher than that in the northwest region. These results were consistent with the results given in Sect. 3.1.1.

The proportion of stations with decreasing trends (43%) was less than that with increasing trends (57%) for CDD (Fig. 4a). Only 1 and 2 stations showed significant increasing and decreasing trends, respectively. Moreover, the regional average CDD time series presented an insignificant decline trend at a rate of − 0.31 days/decade (Fig. 5a). The temporal trends showed that 40 of 44 stations (91%) gave decreasing trends for CWD (Fig. 4b), with only five of them were significant. This can also be seen in the insignificant decline trend of regional average CWD time series (− 0.15 days/decade, Fig. 5b). All stations exhibited negative trends of R0.1mm, of which 35 stations (80%) were significant (Fig. 4c). Over the whole study area, we observed that the R0.1mm significantly decreased at a rate of − 3.04 days/decade (Fig. 5c). For R10mm, more stations exhibited decreasing trends, with only five of them being significant (Fig. 4d). Moreover, the

regional R10mm time series significantly decreased (− 0.32 days/decade) (Fig. 5d). The number of stations showing decreasing trends (75%) was also more than that with increasing trends (25%) for R12mm (Fig. 4e). However, the regional R12mm time series gave an insignificant decline trend at a rate of − 0.24 days/decade (Fig. 5e). As for R25mm, the number of stations giving decreasing trends was the same as that giving increasing trends (Fig. 4f). This can also be seen in the regional average R25mm time series that an insignificant decline trend at a rate of − 0.02 days/decade can be detected in Fig. 5f.

The values of most indices (except CDD) increased from the northwest to the southeast of the MRYRB, which was consistent with the spatial variation of annual precipitation in this area, revealing that the southeast region was the wettest region, whereas the northwest region was relatively dry in the MRYRB. These results were consistent with the previous studies in the similar regions, such as Liu et al. (2008) and Sun et al. (2016). In the MRYRB, we have not found any evidence of disproportionately large increase in the precipitation extremes, which have been revealed in the global (Alexander et al., 2006) and many other regions (Wang et al., 2013; Limsakul and Singhruck, 2016). The trend of regional average PRCPTOT was insignificant negative at the 95% confidence level. Except the significant decreasing trends exhibited in R0.1mm and R10mm, no significant changes were observed in the annual regional average series of other extreme precipitation indices. The trends in the extreme precipitation indices indicated that the MRYRB was becoming drying with less frequent precipitation events, which was consistent with the results given by Liu et al. (2008) and Zhang et al. (2014). Moreover, You et al. (2011) revealed that the magnitude of negative changes at the stations in the Yellow River Basin is larger than the other regions in China. Zhang et al. (2014) revealed that there is an evident decline in the precipitation in the Yellow River Basin, particularly in the MRYRB; such decline is mainly caused by the decrease in precipitation amount and rainy days. Changes in extreme precipitation events play an important role in the generation of floods. Significant increasing trends in extreme precipitation can be observed in many large river basins in China, such as the Yangtze River Basin (Chen et al., 2013) and Songhua River Basin (Song et al., 2015), which may result in more severe flood disasters in these areas. However, in our study area, no significant change can be observed in these considered indices, which may suggest that the risk of flood disaster in this area may also have few changes. Besides, the significant decreasing trend of regional R0.1mm series may accompany with aggravation of droughts in the whole region, which can partly explain why the Yellow River always suffered from severe drought and occurrence of flow-break during recent decades (Cong et al. 2009). Moreover, the insignificant decline of regional R12mm suggested probable mitigation of soil erosion. Simultaneously, many previous studies have proved that the reduction of soil erosion and sediment transported in the Yellow River is due to climate change (decrease of precipitation) and human activities (such as landscape engineering, terracing, and the construction of check dams) (Xu, 2004; Wang et al., 2007; Wang et al., 2015).

3.2 The statistical characteristic of extreme precipitation series

3.2.1 Selection of best fit distribution

In this study, the GEV, GP, and gamma distributions were used to fit the extreme precipitation time series of all indices in the MRYRB during 1960–2013. The optimal model was determined using the KS test at the confidence level of 0.95. The results were summarized in Tables 4 and 5. On the station scale, the GEV distribution can be accepted as the optimal choice for most occasions. This was also proved by the results at the regional scale. GEV distribution can best simulate the regional time series of all indices except R12mm, of which Gamma was proved to be the optimal distribution. However, the KS statistics of the GEV and gamma distribution were quite close, and both of them have passed the KS test at the confidence level of 0.95. These results indicated the efficiency of GEV in modeling of extreme precipitation time series in our study area. In fact, GEV distribution has been reported to be the best fit model in many regions by the comparison with other extreme value distributions, e.g., Fischer et al. (2012). It is worth noting that, although the GP distribution was widely used in many studies (Bhunya et al., 2013; She et al., 2015) to

Table 4 The Kolmogorov-Smirnov test values of extreme precipitation indices series

Index	Regionally averaged value			Best distribution
	GEV	GPD	GAMMA	
CDD	0.060	0.125	0.085	GEV
CWD	0.072	0.079	0.084	GEV
PRCPTOT	0.074	0.152	0.094	GEV
R0.1 mm	0.076	**0.277**	0.111	GEV
R10mm	0.051	0.096	0.061	GEV
R12mm	0.062	0.174	0.060	Gamma
R25mm	0.050	0.131	0.062	GEV
R95	0.061	**0.256**	0.071	GEV
R99	0.055	**0.235**	0.072	GEV
RX1day	0.073	0.095	0.102	GEV
RX5day	0.061	0.089	0.068	GEV
SDII	0.052	**0.271**	0.062	GEV

The bold front in Table 4 represents that the distribution has not passed the 0.95 confidence level

simulate the extreme precipitation time series, it was found to be the worst choice in our study. At station scale, the KS statistic showed that many GP distributions cannot pass the KS test, especially for fitting CWD, R0.1mm, and R25mm. Furthermore, none of the indices showed that the GP distribution was the optimal distribution at the regional scale. To sum up, considering the wide acceptance of the GEV distribution at regional and station scale, we employed this distribution to analyze the statistical characteristic of extreme precipitation in the study area.

3.2.2 The return levels of various indices

According to the best fit distribution results given in Sect. 3.2.1, extreme precipitation indices in each individual station under return period of 50 years were calculated (Fig. 6). As shown in Fig. 6, the spatial distributions of extreme precipitation indices under the return period of 50 years were similar to the spatial patterns of corresponding extreme precipitation indices during 1960–2013, which indicated the rationality to use the GEV distribution to simulate extreme precipitation indices in the MRYRB. The majority of the highest values of these indices (except CDD, of which high value means dry) were distributed in the southeastern region, while most of the lowest values of indices were located in the northwest region. These results confirmed the results in Sects. 3.1.1 and 3.1.2 that the southeastern region was relatively wet, whereas the northwestern region was relatively dry in the MRYRB. The spatial variation of the return level revealed that the risk of extreme precipitation was highest in the southeast of the MRYRB. Therefore, more engineering and non-engineering measures are needed to reduce the losses of extreme precipitation in this region.

3.2.3 Changes in the extreme precipitation in different subperiods

To further examine the temporal changes in the precipitation extremes, we divided the whole time series into two subseries with the same length, i.e., the time period from 1960 to 1986 and from 1987 to 2013. Then, the GEV distribution, which was determined as the optimal distribution in the previous section, was chosen to fit the two subseries, and the changes in the probability distribution functions (PDFs) were given in Fig. 7. The black and red lines represent the annual PDFs in 1960–1986 and 1987–2013, respectively. The shaded area denotes the 5 and 95% cumulative percentages' values.

The PDFs of R25mm, R95, R99, and RX1day changed a little in the two subperiods, which indicated that changes in these indices were quite small during the past several decades. The PDFs of CDD, CWD, PRCPTOT, R10mm, R12mm, RX5day, and SDII moved to the left during the recent several decades. For example, as for the CDD, the 95th percentile during 1960–1986 corresponded to 77.6 days/year, while the 95th percentile during 1987–2013 corresponded to 63.3 days/year (Fig. 7a). The 95th percentile in CWD during 1960–1986 corresponded to 9.0 days/year, while the 95th percentile in CWD during 1987–2013 corresponded to 6.47 days/year (Fig. 7b). The PDF of R0.1mm after 1987 roughly moved to the left; however, the part exceeding the 95th percentile moved to the right. The fifth percentile in R0.1mm during 1960–1986 corresponded to 80.8 days/year, while the fifth percentile during 1987–2013 corresponded to 74.6 days/year; the 95th percentile during 1960–1986 corresponded to 110.0 days/year, while the 95th percentile during 1987–2013 corresponded to 126.0 days/year (Fig. 7d). All in all, general distribution changes in extreme precipitation indices showed a tendency toward drier conditions, which was in accordance with the result of trends analysis in the previous sections.

3.3 Relationship between extreme precipitation indices and large-scale atmospheric circulation

Large-scale atmospheric circulation is an important factor influencing global climate and shows strong correlations with extreme precipitation events in many regions of the word (Sun et al., 2015; Zhang et al., 2016; Jiang et al., 2017). Therefore, analyzing the relationship between extreme precipitation indices and large-scale atmospheric circulation in the MRYRB is significant. Both PDO and ENSO events have shown strong relations with extreme precipitation events, as observed worldwide (Krichak et al., 2014; Limsakul and Singhruck,

Table 5 The numbers of optimal distributions and unqualified distributions

Index	GEV		GP		Gamma	
	x_1	x_2	x_1	x_2	x_1	x_2
CDD	36	0	5	1	3	0
CWD	27	6	11	25	6	13
PRCPTOT	39	0	2	3	3	0
R0.1mm	42	0	0	18	2	0
R10mm	37	0	3	8	4	0
R12mm	35	0	2	9	7	0
R25mm	31	0	6	14	7	5
R95	41	0	1	1	2	0
R99	36	0	6	4	2	0
RX1day	38	0	5	0	1	0
RX5day	37	0	7	2	0	0
SDII	40	0	1	6	3	0

x_1 represents the numbers of optimal distribution stations in the KS test, while x_2 represents the numbers of stations that have not passed the KS test

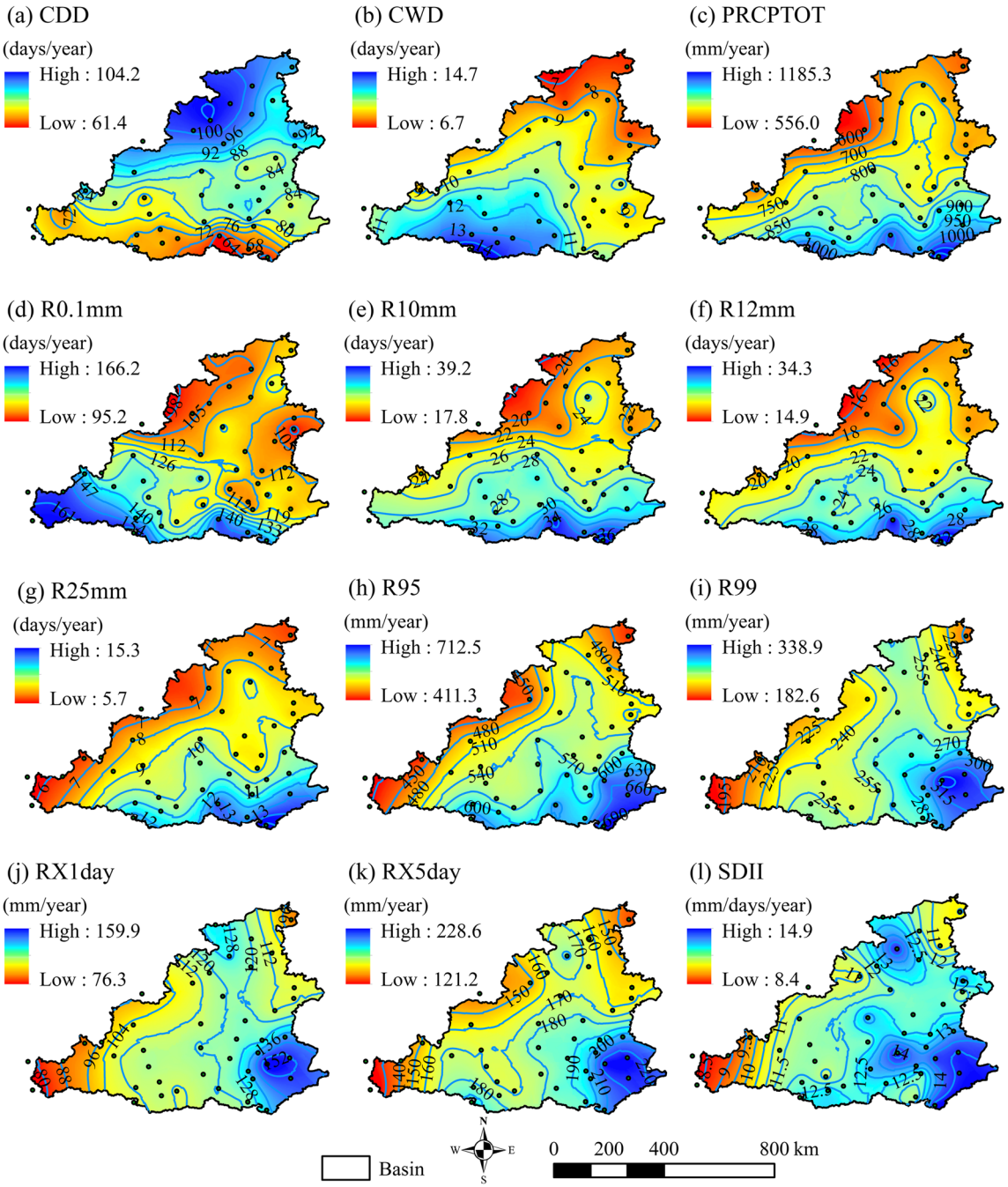

Fig. 6 The quantiles of the indices under the 50-year return period using the GEV distribution

2016; Liu et al., 2017). Here, the cross wavelet analysis was applied to study the connections between ENSO and PDO and extreme precipitation indices (Figs. 8 and 9). For the sake of convenience, we only selected RX1day, R25mm, and CWD which represented the intensity, frequency, and duration of precipitation extremes, respectively, to describe. More details of the cross wavelet transforms between ENSO/PDO and other indices can be found in Figs. 8 and 9.

Figure 8 exhibited the cross wavelet transforms between ENSO and precipitation extremes in the MRYRB. Figure 8j illustrated that the ENSO events showed a statistically significant negative correlation with the RX1day variation with a 2–4-year signal at the 95% confidence level from 1964 to 1970. In addition, ENSO events had a statistically significant positive correlation with the RX1day with a 13–14-year signal at the 95% confidence level from 1983 to 1994. The results indicated that ENSO events played an important role in triggering intensive precipitation in the MRYRB. Figure 8g indicated that the ENSO had a statistically significant negative correlation with R25mm variation in the MRYRB at the

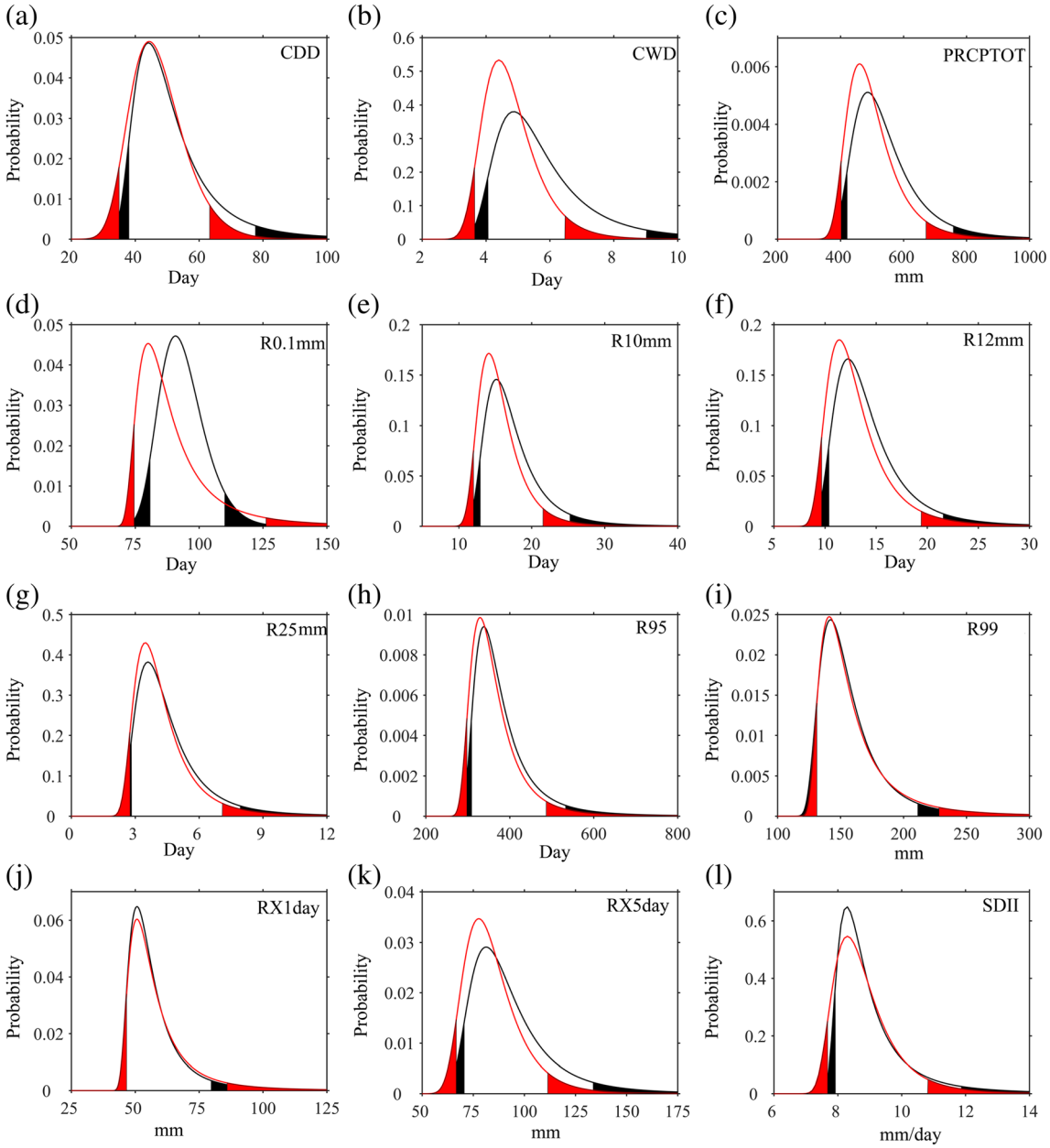

Fig. 7 Annual PDFs of regional average extreme precipitation indices in 1960–1986 (black line) and 1987–2013 (red line). The part for exceeding the 95th percentile and the part for falling under the fifth percentile are considered

95% confidence level, with a 2–4-year signal from 1964 to 1973 and a 3–6-year signal from 1983 to 1993. Moreover, ENSO had a statistically significant positive correlation with the R25mm with an 8–9-year signal at the 95% confidence level from 1999 to 2002. This implied that the ENSO was closely related to the frequency of extreme precipitation events in this area. Figure 8b demonstrated that the ENSO had a statistically significant negative correlation with CWD variation at the 95% confidence level, with a 2–5-year signal from 1980 to 1990, suggesting that the ENSO was closely associated with long-lasting rainy days in the MRYRB.

The cross wavelet transforms between PDO and precipitation extremes in the MRYRB were displayed in Fig. 9. Obviously, the PDO exhibited a statistically negative correlation with RX1day in the MRYRB with a 1–2-year signal from 1998 to 2000 and a positive correlation with a 7–10-year signal from 1996 to 2002 and a 2–4-year signal in 2007–2009 at the 95% confidence level (Fig. 9j). Similarly, Fig. 9g showed that the PDO exhibited a statistically significant negative correlation with R25mm variation in the MRYRB with a 5–6-year signal at the 95% confidence level from 1987 to 1991 and a positive correlation with a 6–10-year signal from 1991 to

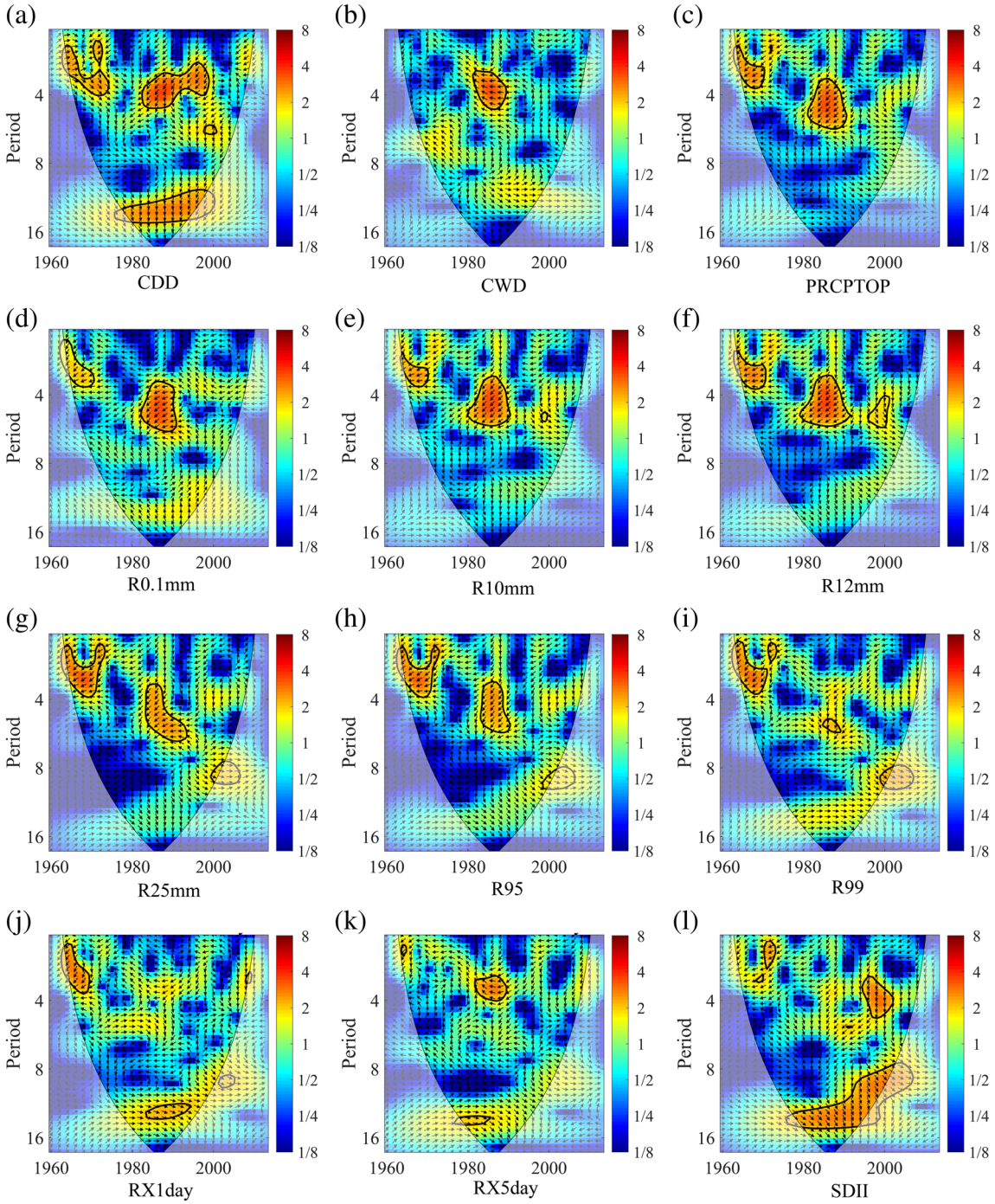

Fig. 8 The cross wavelet transforms between the ENSO and extreme precipitation indices in the MRYRB. The thick black contour denotes the relations which are significant at the 95% confidence level against the red noise. The cone of influence (COI) where edge effects might distort the picture is shown as lighter shades. The relative phase relationship is indicated by the arrow direction (with anti-phase pointing left, in-phase pointing right). The color bar on the right denotes the wavelet energy

2003. Figure 9b illustrated that the PDO showed a statistically significant negative correlation with the CWD variation in the MRYRB with a 2–3-year signal at the 95% confidence level from 1981 to 1984 and a 10-year signal from 1981 to 1992 at the 95% confidence level. In addition, PDO had a statistically significant positive correlation with the CWD with a 2-year signal at the 95% confidence level from 1999 to 2000. These findings indicated that the PDO also had a strong association with changes in the intensity, frequency, and duration extreme precipitation events in the MRYRB.

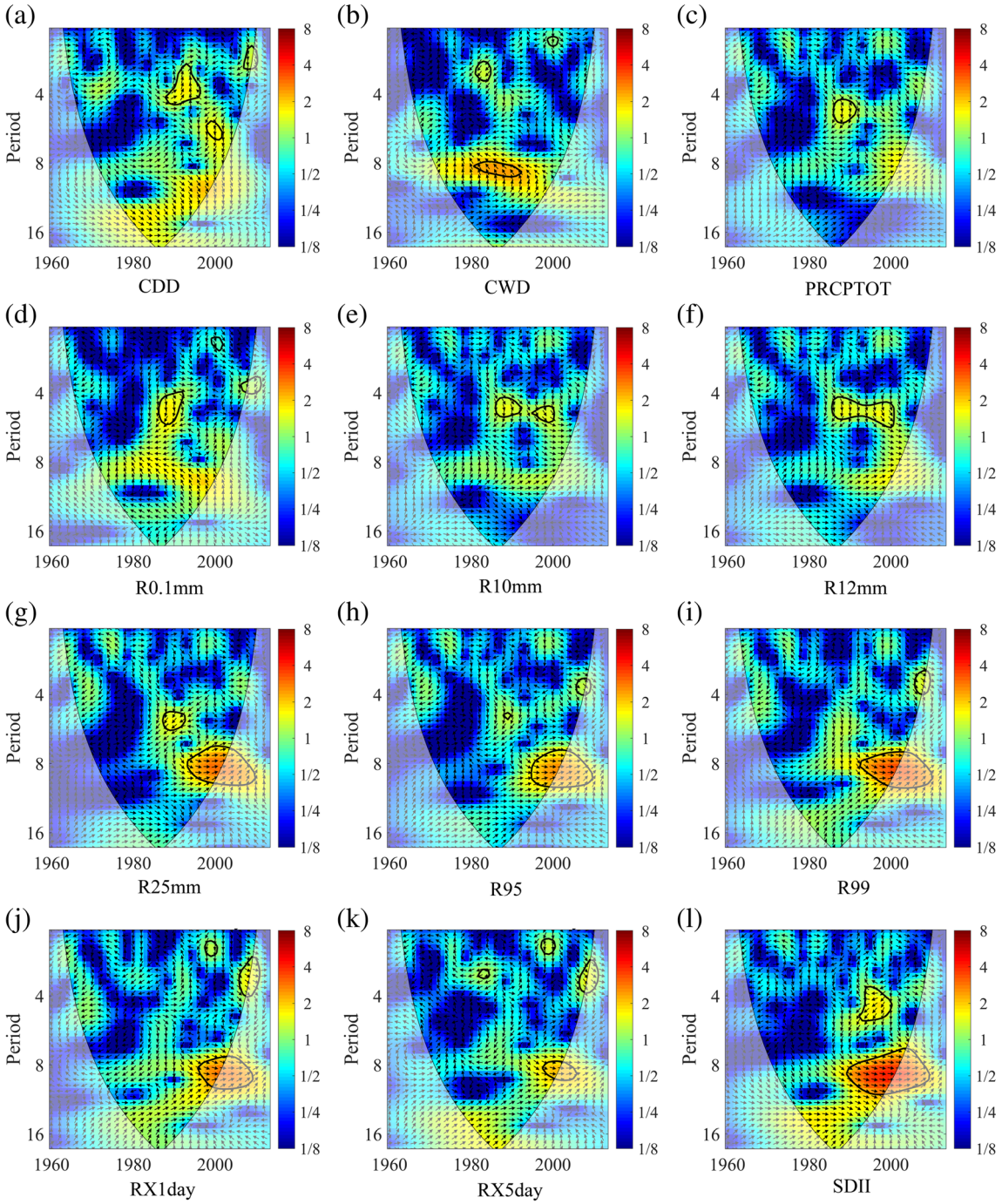

Fig. 9 Same as Fig. 8, but for PDO events

Figures 8 and 9 showed that both ENSO and PDO had statistically evident correlations with precipitation extremes in the MRYRB, indicating that both ENSO and PDO had a strong influence on precipitation extremes. This result is in accordance with Liu et al. (2017). The study of Ouyang et al. (2014) has revealed that precipitation in the major of China decreases during El Niño/PDO warm phase periods and increase during La Niña/PDO cool phase periods. Moreover, the relationships between the extreme precipitation indices and the ENSO and PDO implied that for the El Niño (La Niña) years and the PDO warm (cool) regimes, the variability in the frequency and magnitude of heavy and more intense precipitation events tended to be reduced (enhanced) (Kenyon and Hegerl, 2010; Limsakul and Singhruck, 2016). Our study further revealed that the relationship between ENSO events and precipitation extremes was more

significant, indicating that ENSO can have a larger influence on the precipitation extremes in the MRYRB compared to PDO. This might be due to the limitations of the relatively short record length and uncertainty from the potential interaction between PDO and ENSO (Kiem and Verdon-Kidd, 2009). PDO can indirectly affect precipitation variability via modulation of ENSO impacts (Verdon et al., 2004; Kiem and Verdon-Kidd, 2009). There is much evidence (Chan and Zhou, 2005; Andreoli and Kayano, 2005) that PDO coupled with ENSO affects precipitation constructively (strong and well defined anomalies), when they are in phase, and destructively (weak and noisy anomalies), when they are out of phase. Moreover, some researchers also used other large-scale atmospheric circulation indices to explore the relationship between extreme precipitation and large-scale atmospheric circulation in this study area (Liang et al., 2015; Zhang et al., 2014; Sun et al., 2016). For example, Liang et al. (2015) indicated that the monthly Rx1day, Rx5day, PRCPTOT, and SDII have significant positive relationships with Northern Hemisphere Subtropical High (NHSH) but significant negative relationships with Northern Hemisphere Polar Vortex (NHPV) in the Yellow River Basin. Sun et al. (2016) found that the Western Pacific Subtropical High Intensity Index (WPSHII) is associated with the drying trend through an increase in the CDD in the Loess Plateau. These studies have verified that the large-scale atmospheric circulation index has the potential to improve the prediction of extreme precipitation in the study region.

4 Conclusion

In this study, based on the daily precipitation data of 44 meteorological stations in the MRYRB during 1960–2013, 12 extreme precipitation indices, which can reflect the magnitude, intensity, and duration of precipitation extremes, were selected to analyze the spatiotemporal variation and statistical characteristic of extreme precipitation in the MRYRB. The main conclusions are given as follows:

(1) Spatially, the values of most indices (except CDD) increased from the northwest to the southeast of the MRYRB, suggesting that it was wetter in the southeast region than the northwest region of the MRYRB. The regional average R0.1mm and R10mm showed significant decreasing trends with rates of − 3.04 and − 0.32 days/decade, respectively. For other indices, insignificant decreasing or increasing trends can be observed. These changes in extreme precipitation indices indicated that the MRYRB presented a drying trend with less frequent precipitation.
(2) The GEV distribution was found to be the optimal statistical distribution for the extreme precipitation indices of the MRYRB. The spatial distributions of extreme precipitation indices under the return period of 50 years were similar to the spatial patterns of corresponding precipitation extreme indices during 1960–2013. Moreover, changes in PDFs of indices for the period of 1960–1986 and 1987–2013 indicated a drying trend in the recent decades.
(3) Both ENSO and PDO had statistically correlations with RX1day, R25mm, and CWD, which demonstrated that the intensity, frequency, and duration of precipitation extremes in the MRYRB. That is to say, both ENSO and PDO had a strong influence on precipitation extremes in the MRYRB. This suggested that the large-scale atmospheric circulation index had the potential to improve the prediction of extreme precipitation in the study region.

Acknowledgements The meteorological data used in this study were provided by the China Meteorological Administration (CMA), which is highly appreciated.

Funding information This study was supported by the National Natural Science Foundation of China (Nos. 41571030 and 41571028), Hubei Province Science and Technology Support Plan (No. 2015BCA290), and the Open Foundation of State Key Laboratory of Hydrology-Water Resources and Hydraulic Engineering (No. 2016490211).

References

Aguilar E, Barry AA, Brunet M, Ekang L, Fernandes A, Massoukina M, Mbah J, Mhanda A, do Nascimento DJ, Peterson TC, Umba OT, Tomou M, Zhang X (2009) Changes in temperature and precipitation extremes in western Central Africa, Guinea Conakry, and Zimbabwe, 1955–2006. J Geophys Res-Atmos 114(D2). https://doi.org/10.1029/2008JD011010

Alexander LV, Zhang X, Peterson TC, Caesar J, Gleason B, Tank AMGK, Haylock M, Collins D, Trewin B, Rahimzadeh F, Tagipour A, Rupa Kummar K, Revadekar J, Griffiths G, Vincent L, Stephenson DB, Burn J, Aguilar E, Brunet M, Taylor M, New M, Zhai P, Rusticucci M, Vazquez-Aguirre JL (2006) Global observed changes in daily climate extremes of temperature and precipitation. J Geophys Res 111(D5). https://doi.org/10.1029/2005JD006290

Andreoli RV, Kayano MT (2005) ENSO-related rainfall anomalies in South America and associated circulation features during warm and cold Pacific decadal oscillation regimes. Int J Climatol 25(15): 2017–2030. https://doi.org/10.1002/joc.1222

Bhunya PK, Berndtsson R, Jain SK, Kumar R (2013) Flood analysis using negative binomial and generalized Pareto models in partial duration series (PDS). J Hydrol 497:121–132. https://doi.org/10.1016/j.jhydrol.2013.05.047

Cai JT, Jiang ZH (2007) Advantages of L-moment estimation and its application to extreme precipitation. Acta Meteorol Sin 20:248–260 (in Chinese)

Chan JCL, Zhou W (2005) PDO, ENSO and early summer monsoon rainfall over South China. Geophys Res Lett 32(8):L08810. https://doi.org/10.1029/2004GL022015

Chen YD, Zhang Q, Xiao MZ, Singh VP, Leung Y, Jiang LG (2013) Precipitation extremes in the Yangtze River Basin, China: regional frequency and spatial–temporal patterns. Theor Appl Climatol 116: 447–461

Choi G, Collins D, Ren GY, Trewin B, Baldi M, Fukuda Y, Afzaal M, Pianmana T, Gomboluudev P, Huong PTT, Lias N, Kwon WT, Boo

KO, Cha Y-M, Zhou YQ (2009) Changes in means and extreme events of temperature and precipitation in the Asia-Pacific network region, 1955–2007. Int J Climatol 29(13):1906–1925. https://doi.org/10.1002/joc.1979

Cong Z, Yang D, Gao B, Yang H, Hu H (2009) Hydrological trend analysis in the Yellow River Basin using a distributed hydrological model. Water Resour Res 45:W00A13. doi:https://doi.org/10.1029/2008WR006852

Du H, Xia J, Zeng SD, She DX, Liu JL (2014) Variations and statistical probability characteristic analysis of extreme precipitation events under climate change in Haihe River Basin, China. Hydrol Process 28(3):913–925. https://doi.org/10.1002/hyp.9606

Duan WL, He B, Takara K, Luo PP, MC H, Alias NE, Nover D (2015) Changes of precipitation amounts and extremes over Japan between 1901 and 2012 and their connection to climate indices. Clim Dyn 45(7-8):2273–2292. https://doi.org/10.1007/s00382-015-2778-8

Fiddes SL, Pezza AB, Barras V (2014) Synoptic climatology of extreme precipitation in alpine Australia. Int J Climatol 35:172–188

Fischer T, BD S, Luo Y, Scholten T (2012) Probability distribution of precipitation extremes for weather-index based insurance in the Zhujiang River Basin, South China. J Hydrometeorol 13(3):1023–1037. https://doi.org/10.1175/JHM-D-11-041.1

Gocic M, Trajkovic S (2013) Analysis of changes in meteorological variable using Mann-Kendall and Sen's slope estimator statistical tests in Serbia. Glob Planet Chang 100:172–182. https://doi.org/10.1016/j.gloplacha.2012.10.014

Griffis VW, Stedinger JR (2007) Log-Pearson type 3 distribution and its application in flood frequency analysis. I: distribution characteristics. J Hydrol Eng 12(5):482–491. https://doi.org/10.1061/(ASCE)1084-0699(2007)12:5(482)

Grinsted A, Moore JC, Jevrejeva S (2004) Application of the cross wavelet transform and wavelet coherence to geophysical time series. Nonlinear Proces Geophys 11(5/6):561–566. https://doi.org/10.5194/npg-11-561-2004

Hosking JRM (1990) L-moments: analysis and estimation of distributions using linear combinations of order statistics. J R Stat Soc B 52:105–124

Hosking JRM, Wallis JR (1997) Regional frequency analysis. Cambridge University Press, Cambridge. https://doi.org/10.1017/CBO9780511529443

IPCC (2013) Summary for policymakers. In Climate Change 2013: the physical science basis. Contribution of Working Group I to the Fifth Assessment Report of the Intergovernmental Panel on Climate Change, Stocker TF, Qin D, Plattner G-K, Tignor M, Allen SK, Boschung J, Nauels A, Xia Y, Bex V, Midgley PM (eds). Cambridge University Press: Cambridge, UK and New York, NY

Jia XX, Shao MA, Zhu YJ, Luo Y (2017) Soil moisture decline due to afforestation across the Loess Plateau, China. J Hydrol 546:113–122. https://doi.org/10.1016/j.jhydrol.2017.01.011

Jiang ZH, Shen YC, Ma TT, Zhai PM, Fang SD (2014) Changes of precipitation intensity spectra in different region of mainland China during 1961–2006. J Meteorol Res 28(6):1085–1098. https://doi.org/10.1007/s13351-014-3233-1

Jiang RG, Xie JC, Zhao Y, He HL, He GH (2017) Spatiotemporal variability of extreme precipitation in Shaanxi province under climate change. Theor Appl Climatol 130(3-4):831–845. https://doi.org/10.1007/s00704-016-1910-y

Kendall M (1975) Multivariate analysis. Charles Griffin, London

Kenyon J, Hegerl GC (2010) Influence of modes of climate variability on global precipitation extremes. J Clim 23(23):6248–6262. https://doi.org/10.1175/2010JCLI3617.1

Kiem AS, Verdon-Kidd DC (2009) Climatic drivers of Victorian streamflow: is ENSO the dominant influence? Austr J Water Res 13(1):17–30

Krichak SO, Breitgand JS, Gualdi S, Feldstein SB (2014) Teleconnection–extreme precipitation relationships over the Mediterranean region. Theor Appl Climatol 117(3-4):679–692. https://doi.org/10.1007/s00704-013-1036-4

Liang L, Zhao LN, Gong YF, Tian FY, Wang Z (2012) Probability distribution of summer daily precipitation in the Huaihe Basin of China based on gamma distribution. Acta Meteorol Sin 26(1):72–84. https://doi.org/10.1007/s13351-012-0107-2

Liang K, Liu S, Bai P, Nie R (2015) The Yellow River Basin becomes wetter or drier? The case as indicated by mean precipitation and extremes during 1961–2012. Theor Appl Climatol 119(3-4):701–722. https://doi.org/10.1007/s00704-014-1138-7

Limsakul A, Singhruck P (2016) Long-term trends and variability of total and extreme precipitation in Thailand. Atom Res 169:301–317. https://doi.org/10.1016/j.atmosres.2015.10.015

Liu Q, Yang ZF, Cui BS (2008) Spatial and temporal variability of annual precipitation during 1961–2006 in Yellow River Basin, China. J Hydrol 361(3-4):330–338. https://doi.org/10.1016/j.jhydrol.2008.08.002

Liu SY, Huang SZ, Huang Q, Xie YY, Leng GY, Luan JK, Song XY, Wei X, Li XY (2017) Identification of the non-stationarity of extreme precipitation events and correlations with large-scale ocean-atmospheric circulation patterns: a case study in the Wei River Basin, China. J Hydrol 548:184–195. https://doi.org/10.1016/j.jhydrol.2017.03.012

Mann HB (1945) Nonparamentric tests against trend. Econometrica 13(3):245–259. https://doi.org/10.2307/1907187

Min S-K, Son S-W, Seo K-H, Kug J-S, An S-I, Choi Y-S, Jeong J-H, Kim B-M, Kim J-W, Kim Y-H, Lee J-Y, Lee M-I (2015) Changes in weather and climate extremes over Korea and possible causes: a review. Asia-Pac J Atmos Sci 51(2):103–121. https://doi.org/10.1007/s13143-015-0066-5

Najafi MR, Moazami S (2016) Trends in total precipitation and magnitude–frequency of extreme precipitation in Iran, 1969–2009. Int J Climatol 36(4):1863–1872. https://doi.org/10.1002/joc.4465

Ouyang R, Liu W, Fu G, Liu C, Hu L, Wang H (2014) Linkages between ENSO/PDO signals and precipitation, streamflow in China during the last 100 years. Hydrol Earth Syst Sc 18(9):3651–3661. https://doi.org/10.5194/hess-18-3651-2014

Sansigolo CA, Kayano MT (2010) Trends of seasonal maximum and minimum temperatures and precipitation in Southern Brazil for the 1913–2006. Theor Appl Climatol 101(1-2):209–216. https://doi.org/10.1007/s00704-010-0270-2

dos Santos CAC, Neale CMU, Rao TVR, da Silva BB (2011) Trends in indices for extremes in daily temperature and precipitation over Utah USA. Int J Climatol 31(12):1813–1822. https://doi.org/10.1002/joc.2205

Sen PK (1968) Estimates of the regression coefficient based on Kendall's tau. J Am Stat Assoc 63(324):1379–1389. https://doi.org/10.1080/01621459.1968.10480934

Sen Roy S, Balling RC (2004) Trends in extreme daily precipitation indices in India. Int J Climatol 24(4):457–466. https://doi.org/10.1002/joc.995

Shao QX, Wong H, Xia J, Ip W-C (2004) Models for extremes using the extended three-parameter Burr XII system with application to flood frequency analysis. Hydrol Sci J 49:685–702

She DX, Shao QX, Xia J (2015) Investigating the variation and non-stationarity in precipitation extremes based on the concept of event-based extreme precipitation. J Hydrol 530:785–798. https://doi.org/10.1016/j.jhydrol.2015.10.029

She DX, Xia J, Zhang YJ, Shan LJ (2016) Regional frequency analysis of extreme dry spells during rainy season in the Wei River Basin. China Adv Meteorol 2016:1–13. https://doi.org/10.1155/2016/6427568

Shi H, Shao MA (2000) Soil and water loss from the loess plateau in China. J Arid Environ 45(1):9–20. https://doi.org/10.1006/jare.1999.0618

Song XY, Song SB, Sun WY (2015) Recent changes in extreme precipitation and drought over the Songhua River Basin, China, during

1960–2013. Atmos Res 157:137–152. https://doi.org/10.1016/j.atmosres.2015.01.022

Su BD, Kundzewicz ZW, Jiang T (2009) Simulation of extreme precipitation over the Yangtze River Basin using Wakeby distribution. Theor Appl Climatol 96:209–219

Sun X, Renard B, Thyer M, Westra S, Lang M (2015) A global analysis of the asymmetric effect of ENSO on extreme precipitation. J Hydrol 530:51–65. https://doi.org/10.1016/j.jhydrol.2015.09.016

Sun WY, XM M, Song XY (2016) Changes in extreme temperature and precipitation events in the Loess Plateau (China) during 1960–2013 under global warming. Atmos Res 168:33–48. https://doi.org/10.1016/j.atmosres.2015.09.001

Torrence C, Compo GP (1998) A practical guide to wavelet analysis. Bull Am Meteorol Soc 79(1):61–78. https://doi.org/10.1175/1520-0477(1998)079<0061:APGTWA>2.0.CO;2

Trenberth KE (1998) Atmospheric moisture residence times and cycling: impactions for rainfall rates and climate change. Clim Chang 39(4):667–694. https://doi.org/10.1023/A:1005319109110

Verdon DC, Wyatt AM, Kiem AS, Franks SW (2004) Multidecadal variability of rainfall and streamflow: eastern Australia. Water Resour Res 40(10):W10201. https://doi.org/10.1029/2004WR003234

Wang XL, Feng Y (2013) RHtestsV4 user manual. Climate Research Division Atmospheric Science and Technology Directorate Science and Technology Branch. Environment Canada, Toronto, Ontario, Canada

Wang H, Yang ZS, Saito Y, Liu JP, Sun XX, Wang Y (2007) Stepwise decreases of the Huanghe (Yellow River) sediment load (1950–2005): impacts of climate change and human activities. Glob Planet Change 57(3-4):331–354. https://doi.org/10.1016/j.gloplacha.2007.01.003

Wang HJ, Chen JN, Chen ZS (2013) Spatial distribution and temporal trends of mean precipitation and extremes in the arid region, northwest of China, during 1960–2010. Hydrol Process 27(12):1807–1818. https://doi.org/10.1002/hyp.9339

Wang S, BJ F, Piao SL, Lv YH, Ciais P, Feng XM, Wang YF (2015) Reduced sediment transport in the Yellow River due to anthropogenic changes. Nat Geosci 9(1):38–41

Wu H, Qian H (2016) Innovative trend analysis of annual and seasonal rainfall and extreme values in Shaanxi, China, since the 1950s. Int J Climatol 37:2582–2592

Xia J, She DX, Zhang YY (2012) Spatio-temporal trend and statistical distribution of extreme precipitation events in Huaihe River Basin during 1960–2009. J Geophys Res 22:195–208

Xie Y, Liu BY, Zhang WB (2000) Study on standard of erosive rainfall. Soil Water Conserv 14:6–11 (in Chinese)

Xu JX (2004) Effect of human activities on overall trend of sedimentation in the lower Yellow River, China. Environ Manag 33:637–653

Yang T, Shao QX, Hao ZC, Chen X, Zhang ZX, CY X, Sun LM (2010) Regional frequency analysis and spatio-temporal pattern characterization of rainfall extremes in the Pearl River Basin, China. J Hydrol 380(3-4):386–405. https://doi.org/10.1016/j.jhydrol.2009.11.013

Yang P, Xia J, Zhang YY, Hong S (2017) Temporal and spatial variations of precipitation in Northwest China during 1960–2013. Atmos Res 183:283–295. https://doi.org/10.1016/j.atmosres.2016.09.014

You QL, Kang SC, Aguilar E (2011) Changes in daily climate extremes in China and their connection to the large scale atmospheric circulation during 1961–2003. Clim Dynam 36(11-12):2399–2417. https://doi.org/10.1007/s00382-009-0735-0

Young IT (1977) Proof without prejudice: use of the Kolmogorov-Smirnov test for the analysis of histograms from flow systems and other sources. J Histochem Cytochem 25(7):935–941. https://doi.org/10.1177/25.7.894009

Yue S, Wang CY (2002) Applicability of prewhitening to eliminate the influence of serial correlation on the Mann-Kendall test. Water Resour Res 38:1068–1074

Zhai P, Zhang X, Wan H (2005) Trends in total precipitation and frequency of daily extremes over China. J Clim 18(7):1096–1108. https://doi.org/10.1175/JCLI-3318.1

Zhang Q, Peng JT, Singh VP (2014) Spatio-temporal variations of precipitation in arid and semiarid regions of China: the Yellow River Basin as a case study. Glob Planet Chang 114:38–49. https://doi.org/10.1016/j.gloplacha.2014.01.005

Zhang Q, Xiao M, Singh VP, Wang Y (2016) Spatiotemporal variations of temperature and precipitation extremes in the Poyang Lake basin, China. Theor Appl Climatol 124(3-4):855–864. https://doi.org/10.1007/s00704-015-1470-6

Zong Y, Chen X (2000) The 1998 flood on the Yangtze, China. Nat Hazards 22(2):165–184. https://doi.org/10.1023/A:1008119805106